LIMNOLOGY and OCEANOGRAPHY

ASLO

Limnol. Oceanogr. 69, 2024, 1187–1203

doi: 10.1002/lno.12561

Strong and efficient summertime carbon export driven by aggregation processes in a subarctic coastal ecosystem

Stephanie H. O'Daly,[1*] **Gwenn M. M. Hennon**,[1] **Thomas B. Kelly**,[1] **Suzanne L. Strom**,[2] **Andrew M. P. McDonnell**[1]

[1]College of Fisheries and Ocean Sciences, University of Alaska Fairbanks, Fairbanks, Alaska, USA
[2]Shannon Point Marine Center, Western Washington University, Anacortes, Washington, USA

Abstract

Sinking marine particles, one pathway of the biological carbon pump, transports carbon to the deep ocean from the surface, thereby modulating atmospheric carbon dioxide and supplying benthic food. Few in situ measurements exist of sinking particles in the Northern Gulf of Alaska; therefore, regional carbon flux prediction is poorly constrained. In this study, we (1) characterize the strength and efficiency of the biological carbon pump and (2) identify drivers of carbon flux in the Northern Gulf of Alaska. We deployed up to five inline drifting sediment traps in the upper 150 m to simultaneously collect bulk carbon and intact sinking particles in polyacrylamide gels and measured net primary productivity from deck-board incubations during the summer of 2019. We found high carbon flux magnitude, low attenuation with depth, and high export efficiency. We quantitatively attributed carbon flux between 10 particle types, including various fecal pellet categories, dense detritus, and aggregates using polyacrylamide gels. The contribution of aggregates to total carbon flux (41–93%) and total carbon flux variability (95%) suggest that aggregation processes, not zooplankton repackaging, played a dominant role in carbon export. Furthermore, export efficiency correlated significantly with the proportion of chlorophyll *a* in the large size fraction (> 20 μm), total aggregate carbon flux, and contribution of aggregates to total carbon flux. These results suggest that this stratified, small-cell-dominated ecosystem can have sufficient aggregation to allow for a strong and efficient biological carbon pump. This is the first integrative description of the biological carbon pump in this region.

Gravitationally sinking marine particles transport photosynthetically fixed carbon from the euphotic zone to the ocean's interior and benthos. Such flux is an important biological carbon pump component, contributing to the global carbon cycle (Kwon et al. 2009; Le Moigne 2019). Despite many decades of studies, there are large uncertainties in our understanding of the biological carbon pump due partly to large temporal and spatial heterogeneity in export flux (Buesseler et al. 2007; Henson et al. 2011; Laufkötter et al. 2016; Kelly et al. 2018). While global biological carbon pump estimates vary by nearly 50%, ranging between 7 and 16 Pg C yr^{-1} (Dunne et al. 2007; Henson et al. 2012; Laufkötter et al. 2016), regional estimates under a changing climate are often even more uncertain. For example, under warming ocean conditions, some models predict more efficient carbon export in high-latitude regions (Weber et al. 2016), such as the Northern Gulf of Alaska, while others predict less efficient carbon export (Henson et al. 2012; Marsay et al. 2015).

The composition of sinking marine particles affects the overall net carbon flux (Turner 2015); therefore, accurately parameterizing rates based on this composition is an important way to improve climate model accuracy (Siegel et al. 2014; Laufkötter et al. 2016). Sinking marine particles can be broadly organized into three functional types: (1) phytoplankton cells, (2) zooplankton fecal pellets, and (3) aggregates of detrital material (Turner 2015). These different types of particles overlap in size, but exist in distinct ranges in composition, density, shape, porosity, and ecological sources (Alldredge 1998; Buesseler et al. 2007; Iversen and Ploug 2010; Turner 2015). These distinctive properties result in different sinking speeds (Armstrong et al. 2002; De La Rocha and Passow 2007; Iversen and Lampitt 2020) and remineralization rates

*Correspondence: shodaly2@alaska.edu

Additional Supporting Information may be found in the online version of this article.

Author Contribution Statement: S.O., S.S., and A.M.: Conceptualization, methodology, and investigation. S.S., A.M., G.H.: Funding acquisition and project administration. S.O., T.K., A.M.: Formal analysis. G.H., T.K., and A.M.: Supervision. S.O.: Visualization, writing—original draft preparation. S.O., G.H., T.K., S.S., and A.M.: Writing—reviewing and editing.

(Ploug et al. 2008*b*; Kobari et al. 2013). Marine particle size has been used to calculate carbon content and to predict sinking speed (Stemmann et al. 2004; Guidi et al. 2008); however, considering only particle size masks potential differences in export among particle types. Understanding the role of particle type in addition to size will help reduce uncertainty in the ocean's biological carbon pump.

In contrast to the biological carbon pump, primary productivity and phytoplankton community composition have been well studied in the Northern Gulf of Alaska. Summers are often characterized by a nutrient-limited community of small-celled nanoflagellates and picoplankton (Strom et al. 2006). Stations closer to the coast are often nitrogen-limited, while stations on the slope are likely iron-limited (Aguilar-Islas et al. 2016). This results in moderate summertime primary productivity rates, similar to other nutrient-limited regions. In contrast, the springtime community is typically characterized by large diatoms and high rates of primary productivity (Strom et al. 2016). Based on the dominance of small phytoplankton cells, high rates of microzooplankton grazing (Strom et al. 2001, 2007) and high macrozooplankton biomasses (Moriarty et al. 2013), we would expect a weak and inefficient summertime biological carbon pump with sinking material dominated by zooplankton fecal pellets. Indeed, relatively large contributions of fecal pellets have been measured in the Southern Ocean, another high-latitude system (Ebersbach and Trull 2008; Laurenceau-Cornec et al. 2015).

As a part of the Northern Gulf of Alaska Long Term Ecological Research program, we used PIT-style (Knauer et al. 1979) sediment traps to measure the quantity and quality of sinking particles in the Northern Gulf of Alaska during June and July 2019, along with corresponding measurements of euphotic zone primary production. In addition, we estimated the contribution of phytoplankton cells, aggregates, and fecal pellets to overall carbon flux using polyacrylamide gel traps. This study characterizes the strength and efficiency of the biological carbon pump across the Northern Gulf of Alaska and the potential drivers of these patterns. This study sets a baseline for the biological carbon pump in the Northern Gulf of Alaska, as these are the first measurements of carbon export in this region of which we are aware, and contributes to our understanding of the broader coastal subarctic.

Materials and methods

Study area and hydrography

The Northern Gulf of Alaska is a productive, high latitude, coastal ecosystem characterized by a cyclonic sub-Arctic gyre. Prevailing winds from the Aleutian Low and freshwater inputs seasonally force downwelling over the shelf (Royer and Emery 1987) and promote upwelling off the shelf within the Gulf of Alaska sub-Arctic gyre (Muench et al. 1978; Macklin et al. 1990; Ladd et al. 2016). The eastern boundary of this gyre is the slower and wider Alaska Current, which turns into the narrower and faster Alaskan Stream near Kodiak Island (Danielson et al. 2022). The Alaska Coastal Current is driven by winds and freshwater inputs and forms a very fast current that hugs the Alaskan coastline on the shelf, also in a cyclonic direction (Reed and Schumacher 1986). The upwelling gyre replenishes macronutrients to the surface waters offshore, resulting in high nutrient/low chlorophyll (HNLC) waters that are typically iron-limited (Aguilar-Islas et al. 2016). The Alaska Coastal Current waters have seasonally high iron inputs from glacial runoff; in summer and fall, primary producers are typically macronutrient-limited due to strong stratification from freshwater input and warming. A shelf break front can form in the vicinity of the 300-m isobath, promoting vertical transport of deeper nutrient-rich waters to the surface (Fig. 1) (Aguilar-Islas et al. 2016; Strom and Fredrickson 2020). As such, productivity can be high along the shelf break where onshore and offshore waters meet (Parsons 1987; Stabeno et al. 2004; Jaeger and Nittrouer 2006). The shelf surrounding Kodiak Island has banks that are shallow enough that tidal energy can mix bottom water to the surface, providing nutrients and breaking down stratification (Mordy et al. 2019), which leads to higher summertime production. As a high-latitude system, the Northern Gulf of Alaska is known for high seasonal and interannual variability in chlorophyll and primary production (Waite and Mueter 2013; Strom et al. 2016), often experiencing a strong spring bloom of large-celled phytoplankton (e.g., diatoms) and a smaller magnitude fall bloom (Sambrotto and Lorenzen 1987; Napp et al. 1996). Summers are characterized by stratification due to solar radiation and freshwater input, resulting in low- to moderate productivity dominated by picophytoplankton and nanophytoplankton (Childers et al. 2005; Weingartner et al. 2005).

Data from this study were collected as part of the Northern Gulf of Alaska Long Term Ecological Research program during the SKQ2019-15S cruise from 30 June to 17 July 2019 on the R/V *Sikuliaq*. Three transects were sampled, including the Gulf of Alaska line (GAK), the Kodiak Island line (KOD), and the Middleton Island line (MID), as well as stations in Prince William Sound (PWS) (Fig. 1; Table 1). Shelf station GAK1 is located near shore and within the Alaska Coastal Current. The rest of the shelf stations (GAK5, MID5, and KOD5) and the shelf break station (GAK9) are not located in a major current, although they may experience advective processes due to mesoscale eddies and episodic wind events. MID10, GAK15, and KOD10 are slope stations located within the Alaska Current/Alaska Stream. PWS2 is located within Prince William Sound and is categorized as a sound station.

Sediment trap, ^{13}C net primary productivity (NPP), and CTD data from this study come from intensive stations (Fig. 1). The CTD unit consisted of a Seabird SBE16plus unit coupled with a WetLabs fluorometer and transmissometer. An Underwater Vision Profiler 5 Standard Definition (UVP5; Hydroptic) unit was mounted to the frame, measured in situ particles from 102 μm to 26 mm, and was deployed with every CTD cast.

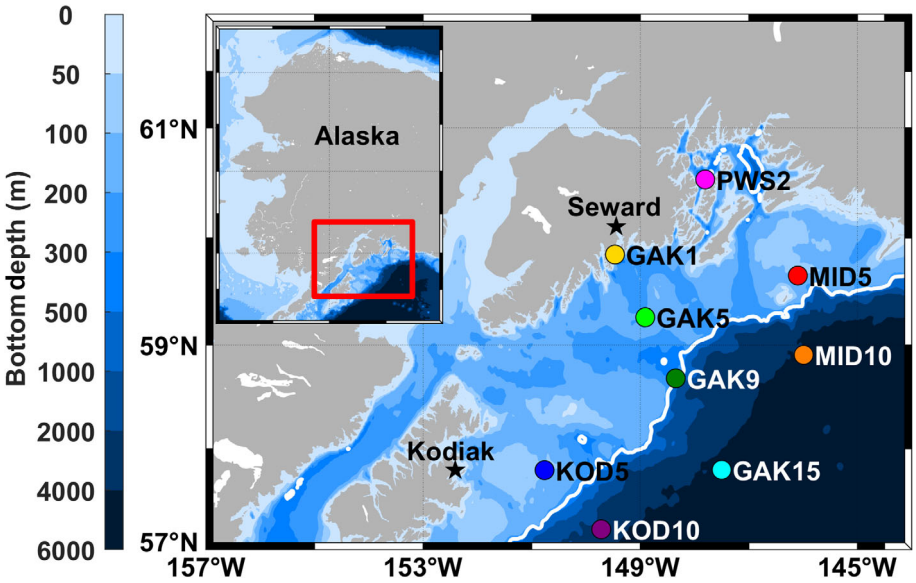

Fig. 1. Locations of process stations where drifting sediment traps were deployed and net primary productivity (NPP) rates were measured (colored circles). The 300 m isobath, which separates the continental shelf from the slope, is shown in white. These stations largely fall on three transect lines, Kodiak Line (KOD), Gulf of Alaska Line (GAK), and Middleton Island Line (MID), as well as a single station in Prince William Sound (PWS).

Sediment trap sampling and analysis

Lagrangian surface-tethered drifting sediment traps (PITs; KC Denmark model number 28.2000) were deployed to collect sinking particles (Moran et al. 2012; O'Daly et al. 2020). Nine stations were sampled with durations between 6 and 19 h (median $\sim$ 10 h) depending on other cruise operations (Table 1). The shallowest crossframe was deployed at approximately 27 m, our best estimate of the base of the euphotic zone (1% light level) in this region during the summer based on previous observations, with each subsequent crossframe tethered in 25 m increments. We sampled between two and five depths depending on the local bathymetry at each deployment (Table 1). The deepest trap for each deployment was positioned at least 20 m above the seafloor to reduce the impacts of benthic resuspension. The depth of the euphotic zone during this cruise averaged 28 m. For export flux estimates, we selected the trap that was closest in depth to the base of the euphotic zone ($\pm$ 9 m) or the trap immediately below the euphotic zone. All mixed layer depths, as identified by a density offset of 0.125 kg m^{-3} (Williams et al. 2006), were less than 20 m, consistent with summer conditions in this region (Sarkar et al. 2005). As such, all traps at each station were deployed below the mixed layer.

Each inline crossframe consisted of four tubes on beveled hinges. Two of the four tubes collected sinking particles in bulk and were partially filled with filtered seawater brine (i.e., 0.22 μm + NaCl, salinity > 50) that was poisoned (i.e., 1% formalin, final concentration, buffered to saturation with borax) and chilled (4°C). The remaining two tubes in each trap array had a removable clear-bottomed cup filled with clear, viscous polyacrylamide gel (50 mL). The cups were fitted with a thin sloping ramp, which created a seal on the inside of the tube walls and funneled sinking particles into the cup. All four tubes were then filled carefully to the top with chilled (4°C) and filtered (0.22 μm millipore sterivex filter cartridges) seawater.

We measured sinking particulate organic carbon (POC) from the bulk trap material as follows. After recovery, each trap tube was covered and left to rest for about 2 h until all sinking particles reached the bottom, then overlying water was removed from all tubes down to a boundary layer of the brine for the bulk tubes or as close to the surface of the gel as possible without disturbing the gel. Gel cups were removed, covered, and stored in the dark until they could be imaged, which occurred < 6 h after recovering the drifting sediment trap (*see* "Gel trap imaging and image processing" for more details). Sinking particles in the two bulk collection tubes at each depth were quantitatively split into 10 subsamples, each using a McLane rotary splitter. All subsamples were passed through a 500 μm mesh to remove swimmers (Owens et al. 2013; Baker et al. 2020). Three subsamples were combined for POC and filtered onto precombusted, preweighed 25-mm Whatman GF/F filters. All filters were dried in a dehydrator at 60°C for 12 h and sealed in Petri dishes until further analysis. This resulted in two POC flux values per trap depth (i.e., one per bulk collection tube).

Carbon samples were processed in the Alaska Stable Isotope Facility at the University of Alaska Fairbanks Water and Environmental Research Center, according to O'Daly et al. (2020). POC/PN filters were acidified with 10% hydrochloric acid for 24 h (fumigation method) to remove inorganic carbon. All sample filters were pelletized in tin cups and processed by a CHN

Table 1. Location, duration, and depth of drifting sediment trap deployments in the Northern Gulf of Alaska.

Sta.	Category	Seafloor depth (m)	Depth of traps (m)	Deploy time (UTC)	Deploy latitude	Deploy longitude	Recover time (UTC)	Recover latitude	Recover longitude	Duration (h)
GAK1	Shelf	269	27, 53, 78, 103, 128	13 Jul 2019 13:00 h	59.829	−149.453	13 Jul 2019 20:50 h	59.816	−149.466	7.8
GAK5	Shelf	173	27, 53, 78, 103	12 Jul 2019 12:47 h	59.245	−148.898	12 Jul 2019 20:18 h	59.254	−148.956	8.5
GAK9	Shelf	270	27, 53, 78, 103, 128	10 Jul 2019 14:07	58.662	−148.342	11 Jul 2019 07:05 h	58.645	−148.350	17.0
GAK15	Slope	4400	27, 53, 78, 103, 128	09 Jul 2019 06:32 h	57.780	−147.476	10 Jul 2019 00:55 h	57.800	−147.455	18.4
KOD5	Shelf	86	27, 53	15 Jul 2019 14:58 h	57.780	−150.760	15 Jul 2019 21:19 h	57.789	−150.899	6.3
KOD10	Slope	2501	27, 53, 78, 103, 128	17 Jul 2019 00:21 h	57.203	−149.721	17 Jul 2019 15:54 h	57.084	−149.738	15.5
MID5	Shelf	93	25, 50	02 Jul 2019 07:31 h	59.65	−146.095	02 Jul 2019 22:11 h	59.652	−146.168	14.7
MID10	Slope	4464	25, 50, 75, 100, 125	03 Jul 2019 13:26 h	58.909	−145.997	03 Jul 2019 21:17 h	58.849	−145.849	7.9
PWS2	Sound	731	80, 105, 130, 155	30 Jun 2019 17:31 h	60.554	−147.793	01 Jul 2019 03:39 h	60.558	−147.769	10.1

elemental analyzer. POC values were converted to daily fluxes (i.e., g C m^{-2} d^{-1}) based on deployment duration and trap area.

An average chemically derived POC flux error (found to be 14%) was calculated as the average normalized variation from the mean of duplicate samples at each depth (Supporting Information Fig. S1; Supporting Information Table S1). Chemically derived POC flux attenuation was calculated using a power-law function shown in Eq. 1 (Buesseler et al. 2007)

$$\frac{F}{F_0} = \left(\frac{z}{z_0}\right)^{-b}, \tag{1}$$

where z is the depth of the trap and z_0 is the depth of the shallowest trap (m for both), F is the flux at depth z, F_0 is the flux at the shallowest trap depth, and b is a unitless exponent that is the best-fit attenuation coefficient. The attenuation coefficient, b, was found by fitting Eq. 1 and minimizing the sum of squared residuals between measured and modeled POC flux using fminsearch in Matlab 2019B.

NPP rate and chlorophyll *a* measurements

Rates of NPP were measured at six depths spanning the euphotic zone using 24 h on-deck incubations (Hama et al. 1983). Water was collected by Niskin rosette, spiked with $H^{13}CO_3^-$ and incubated in screened bags corresponding to in situ collection irradiance (range 100% to 1% of surface irradiance as estimated from the PAR attenuation coefficient determined during the downcast). After 24 h, each incubation was filtered onto precombusted GF/F filters and frozen at −80°C. Back in the lab, samples were acidified (fumed) with 10% hydrochloric acid for 24 h to remove PIC, pelletized, and sent to the UC Davis Stable Isotope Facility for determination of carbon content and ^{13}C isotopic abundance. Rates were integrated over the depth of the euphotic zone to determine integrated NPP (i.e., mg C m^{-2} d^{-1}). Total integrated and size-fractionated chlorophyll *a* (Chl *a*) was measured as in Strom et al. (2016) and integrated to 75 m, which has been shown to include the bulk of the chlorophyll in the water column in this region during all seasons.

Gel trap imaging and image processing

Polyacrylamide gels containing intact sinking particles were imaged in darkfield illumination with oblique lighting from multiple angles, according to O'Daly et al. (2020). A ruler positioned at the same height as the surface of the gel was imaged using the same settings for each gel to calculate pixels per centimeter for each imaged gel. Gel images were cropped to remove lighting artifacts and jar edges before being processed to detect particles, according to Durkin et al. (2021), with a few modifications (Fig. 2A). Image processing methods were modified to better select particles and minimize false-positive selections. Background determination followed the regional maxima method using the *skimage.morphology.reconstruction* function in Python to create a background image, which was

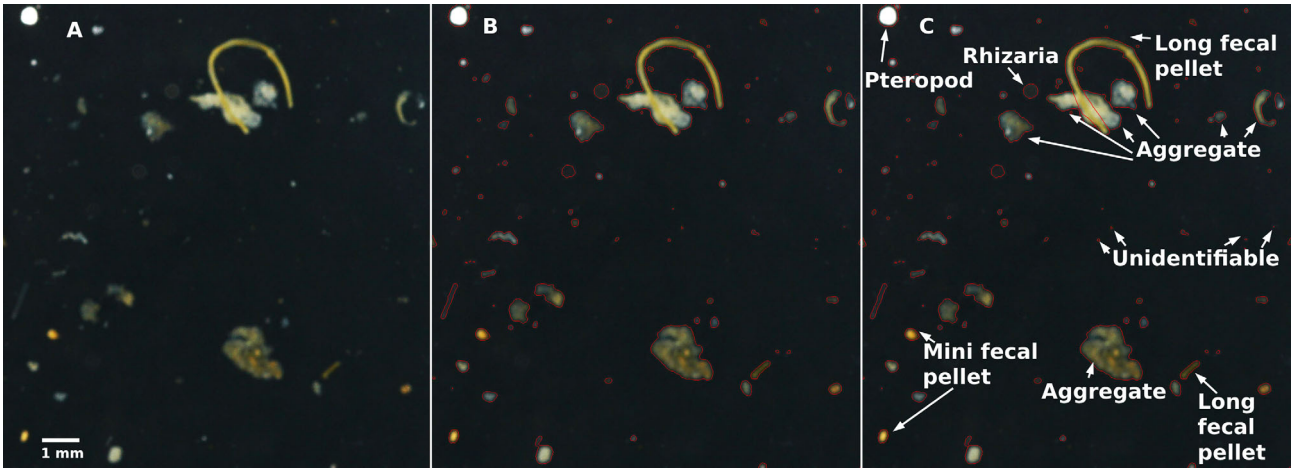

Fig. 2. Particle segmentation and identification. (**A**) Sinking particle in polyacrylamide gel imaging, (**B**) automatic segmentation, (**C**) manual correction to segmentation, and classification. Particles identified as pteropods and other living zooplankton except for rhizaria were removed from carbon calculation. Image enhanced for clarity.

subtracted from the original image. Edge detection was used before thresholding to identify and label in-focus particle edges. In the brightness threshold step, the triangle method was used to select the best thresholding value for each image, rather than a fixed thresholding value, by using the *skimage.filters.threshold_triangle* function. Binary processed images were saved as JPEGs (Fig. 2B) and loaded into Adobe Photoshop CS6 for manual validation. Particles that were incorrectly segmented were manually corrected. The image was then saved and reloaded into the Python routine. A one-pixel erosion step was added before identifying and matching in-focus particle edges to remove a halo effect around particles. Finally, particles were counted and measured (Fig. 2C). Calculating particle fluxes in units of # m^{-2} d^{-1} occurred by grouping particles by their equivalent spherical diameter (ESD) into logarithmically spaced size bins with edges at $\left(2^{\frac{k}{3}}\right)\Big|_{k=10}^{43}$ μm (Durkin et al. 2021). Uncertainty was calculated assuming a Poisson distribution in particle counts.

Gel trap carbon content by particle type

Particles were categorized into 10 different particle types (Fig. 2C): aggregates, dense detritus, long fecal pellet, large loose fecal pellet, short fecal pellet, salp fecal pellet, mini pellet, rhizaria, phytoplankton, and unidentifiable as in Durkin et al. (2021). Rhizaria were included in the carbon flux modeling because most rhizaria can be considered part of the gravitational flux (Bernstein et al. 1987; Michaels et al. 1995; Lampitt et al. 2009). All mesozooplankton were identified in images but removed from consideration when modeling carbon flux from the identified particles because they were assumed not to be part of the gravitational sinking flux. Particles manually identified from GAK15 were used as a training set in a model to predict the type of the remaining particles using high-level Keras preprocessing utilities from the Tensorflow package in Python to speed up the manual validation of all particles. Identification becomes more challenging as particle size decreases. More than 90% of particles smaller than 100 μm were unidentifiable, while only $\sim$ 23% of particles larger than 100 μm were unidentifiable.

We calculated the carbon content for each particle type using a hybrid of inverse modeling and published values depending on particle type. Particle volume was calculated from ESD using type-specific ESD to volume relationships (Supporting Information Table S2) (Durkin et al. 2021). Then particle volumes were converted to carbon using Eq. 2 where C is the calculated carbon content per particle (mg C), A is a scaling coefficient (mg C μm^{-3}), V is the calculated particle volume (μm^3), and B is a unitless exponent parameter.

$$C = A \times V^B. \tag{2}$$

Aggregates and unidentifiable particles were assumed to have the same A (A_{agg}) and B (0.8) values (Menden-Deuer and Lessard 2000; Durkin et al. 2021). Dense detritus, large loose fecal pellets, long fecal pellets, short fecal pellets, and mini fecal pellets were assumed to have the same A value (A_{FP}) and a B value of 1 (Wilson et al. 2008; Durkin et al. 2021). Ideally, each particle type would fit with an individual particle type-specific scaling coefficient, A, and exponent parameter, B, in the model. However, there was not enough data to accurately constrain the model with the increased degrees of freedom, which decreased the overall model certainty. Therefore, we combined particle types to share a scaling coefficient and exponent parameter that we believed would have similar carbon content per unit volume. We grouped unidentifiable particles with aggregates because unidentifiable particles are most likely to be small aggregates. After all, fecal pellets have a biological creation mechanism that prevents them from being infinitely small (likely having a right-skewed relationship with

ESD), whereas aggregates are created physically and, therefore, are more likely to have a log-linear relationship with ESD. In addition, unidentifiable particles are unlikely to substantially influence the overall carbon distributions by type regardless of the scaling coefficients used because they make up a small percentage of total particle volume (0.5–37.5%, averaging 6.4%). Using the same A and B values as aggregates, these values were scaled slightly up when converted to units of carbon where the total percent unidentified carbon flux ranged from 2% to 27% and averaged 8%. In addition, we grouped all the fecal pellets with dense detritus, as has been done in previous studies (Durkin et al. 2021). Dense detritus would have different scaling coefficients than aggregates because they are more tightly packed than aggregates. Again, this choice likely had little outcome on the overall carbon distributions by type because dense detritus made up a small percentage of the total particle volume (0–6.4%, averaging 1.1%). In future studies, having more bulk chemical carbon flux and gel-estimated carbon flux pairs would allow for more individualized scaling values for more particle types.

B values less than one are consistent with less efficient packaging of larger particles (Alldredge 1998). This pattern is more pronounced for aggregates and unidentifiable particles than fecal pellets since aggregate formation allows for large, loosely packed particles (Johnson et al. 1996), while fecal pellets exhibit a more uniform carbon density (Bishop et al. 1980, 1986). Empirically derived or modeled A and B values were used for salp fecal pellets (Silver and Bruland 1981; Iversen et al. 2017), rhizaria (Menden-Deuer and Lessard 2000; Stukel et al. 2018), and phytoplankton (Menden-Deuer and Lessard 2000). Two parameters (i.e., A_{agg} and A_{FP}) were fit to 26 observations.

A maximum likelihood approach (i.e., Markov chain Monte Carlo) was used to fit the log-transformed carbon fluxes to the image-based analysis, yielding both best-fit values and uncertainty (van Oevelen et al. 2010; Yingling et al. 2022). The *optimize.fmin* function in Python was used to determine starting values for the Markov chain Monte Carlo. A stepping scale value of 1e−11 and an exponent scale of 5 were used for both A_{agg} and A_{FP}, which resulted in a reasonable percent acceptance rate of 65.7%. After burn-in, a final solution set containing 100,000 parameterizations was analyzed. The median of these values is considered the best-fit value. Uncertainty is reported as the 95% confidence interval around the median value (Supporting Information Fig. S2).

Images of 26 gels were analyzed to identify particles and calculate gel-derived carbon flux estimates. Due to time restrictions, not every gel image could be analyzed. Priority was given to the GAK line as it is the most well-studied portion of our study area. Gel images from each depth at GAK15 were analyzed in duplicate to determine the amount of variance between tubes. We determined variation was low and only one image per depth was analyzed for the rest of the station-depth pairs. One gel image was analyzed from each depth for the rest of the GAK line. To get a good representation of chemically derived POC flux endmembers, one gel image from KOD5 at 27 m and one gel image from KOD10 at 53 m were analyzed, as these were the samples with the highest chemically derived POC flux without particle overloading in the gel image. In addition, Stas. MID5 and PWS2 had POC flux that increased with depth, which may be a sign of non-steady state conditions: high lateral advection or resuspension from the seafloor. These stations were excluded from image processing for these reasons. The gel-derived carbon flux estimates were within the expected uncertainty of the chemically derived carbon flux values, as most of the spread in the data is within the 2 : 1 and 1 : 2 lines (Supporting Information Fig. S3; Supporting Information Table S3) (Durkin et al. 2021).

Particle concentration size distribution and sinking velocity

The UVP was used to calculate particle concentrations and size distributions throughout the water column. Particles from 102 μm to 26 mm were grouped into 5 m depth bins and one of 25 logarithmically spaced size bins with edges at $\left(2^{\frac{k}{3}}\right)\Big|_{k=18}^{43}$ μm. We calculated depth-specific particle abundance by dividing the number of particles per depth bin by the volume of water imaged per depth bin (#/L).

Size-specific average sinking velocity was calculated by dividing the flux of particles in each overlapping size bin by the concentration of particles in each overlapping size bin (Eq. 3)

$$v = \frac{N_{flux}}{N_{conc}}, \tag{3}$$

where v is the size-specific sinking velocity (m d^{-1}), N_{flux} is the number flux of particles in a size bin (# particles in a size bin m^{-2} d^{-1}) from the gels, and N_{conc} is the number concentration of particles in a size bin (# particles in a size bin m^{-3}) from the UVP. This method averages the sinking velocity for all particles (sinking and suspended) in each size bin and can be thought of as apparent size-specific sinking velocity. Efforts were made to ensure inter-compatibility between the UVP and gel imaging systems so that a given particle would be assigned the same ESD by the UVP and gel imaging systems. We recognize that each system may have individual biases or offsets relative to the other. We note, however, that the particle size spectra from both systems displayed a high degree of autocorrelation within each sample giving us confidence that systematic offsets, if present, would not strongly bias our results.

Statistical analysis

A principal component analysis (PCA) was performed to compare stations by particle abundance and composition. The covariance matrix was calculated using the function *PCA* in the FactoMineR package in R. Quantitative supplementary

variables calculated at each station were plotted in the same space. Variables included gel-estimated carbon flux (Est. C flux), chemically derived carbon flux (Chemical C flux), UVP-derived number concentration averaged from the 50 m above the trap (Total # concen), gel-derived number flux in (Total # flux), average UVP- and gel-derived sinking velocity averaged across sizes (Avg. sinking velocity; Eq. 3), relative contribution of fecal pellet carbon flux (% FP flux), chemically derived carbon to gel-derived volume ratio (C : V ratio), slope of the gel-derived particle size distribution of sinking particles (Slope of PSD) calculated as the linear slope of the number flux vs. size in each gel trap, depth of the trap (depth), and average sinking particle size (Mean size) calculated as the average particle size from each gel.

Results and discussion

Net production of carbon in the euphotic zone

We measured NPP to determine the near-term input of carbon to the system. NPP was variable, ranging from a low of 240 mg C m^{-2} d^{-1} in Prince William Sound (PWS2) to a high of 946 mg C m^{-2} d^{-1} near the shelf break (GAK9) (Table 2). NPP increased with distance from shore on the GAK lines and MID lines (Figs. 3, 4; Table 2). This is expected in summer, as higher rates of NPP are often observed at the shelf break where high iron coastal waters meet high nitrogen offshore waters. Observed NPP values and chlorophyll concentrations were typical for the Northern Gulf of Alaska during summer (Strom and Fredrickson 2020), despite significantly higher sea surface temperatures and greater abundances of small nanoflagellates and picophytoplankton during the summer of 2019 than typically observed (Cohen 2022).

Overall, NPP estimates in the Northern Gulf of Alaska averaged 603 ± 263 mg C m^{-2} d^{-1}, ± 1 SD (Fig. 3A; Table 2). For comparison, summer measurements in the offshore and HNLC North Pacific at Ocean Station Papa (50°N, 145°W) were similar to or less than the Northern Gulf of Alaska: ~ 160 mg C m^{-2} d^{-1} (Estapa et al. 2021), 700 mg C m^{-2} d^{-1} (Buesseler and Boyd 2009), and 300–1500 mg C m^{-2} d^{-1} (Welschmeyer et al. 1993). We would expect similar summertime NPP at Ocean Station Papa and the Northern Gulf of Alaska because both systems are nutrient-limited at this time, the former by dissolved iron and the latter by macronutrients, and both are characterized by communities of picophytoplankton and nanophytoplankton (Booth et al. 1993; Welschmeyer et al. 1993; Strom et al. 2006). When compared to a more productive, coastal, upwelling region, the California Current Ecosystem (32–35°N, 120–124°W) has an average summertime NPP similar to the Northern Gulf of Alaska (747 ± 595 mg C m^{-2} d^{-1}, ± 1 SD) yet with a maximum NPP more than twice that of the maximum measured in the Northern Gulf of Alaska (2333 mg C m^{-2} d^{-1}) (California Current Ecosystem LTER and Goericke 2022). This is indicative of more stable summertime productivity in the Northern Gulf of Alaska than in the California Current Ecosystem. *See* Supporting Information for a description of how the meta-analysis of the California Current Ecosystem data was conducted.

Strength of the biological carbon pump

To determine the strength of the biological carbon pump in the Northern Gulf of Alaska, we deployed sediment traps at nine locations ranging over the continental shelf and slope during the summer of 2019 (Fig. 1; Tables 1, 2). Overall, POC export flux was high, ranging from 158 to 1039 mg C m^{-2} d^{-1} and averaging 390 ± 265 mg C m^{-2} d^{-1} (± 1 SD) (Table 2). The magnitude of POC export flux varied considerably by station but was generally higher near the coast and diminished offshore (Table 2). POC export flux at the shelf stations ranged from 158 to 1039 mg C m^{-2} d^{-1} and averaged 408 ± 324 mg C m^{-2} d^{-1} (± 1 SD) (Table 2). Meanwhile, POC export flux at the slope stations ranged from 232 to 482 mg C m^{-2} d^{-1} and averaged 353 ± 125 mg C m^{-2} d^{-1} (± 1 SD). Along the GAK and KOD lines at all depths, there was a clear decrease in the magnitude of POC flux progressing offshore.

Table 2. Net primary productivity, total integrated chlorophyll *a*, fraction of chlorophyll *a* > 20 μm, particulate organic carbon (POC) export flux, and export ratios at nine stations in the Northern Gulf of Alaska.

Sta.	Euphotic zone depth (m)	Export trap depth (m)	Net primary productivity (mg C m^{-2} d^{-1})	Total integrated chlorophyll *a* (mg m^{-2})	Fraction of chlorophyll *a* > 20 μm	POC export flux (mg C m^{-2} d^{-1})	Export ratio
GAK1	25	27	423	27.4	0.32	398±56	0.94±0.13
GAK5	29	27	614	17.5	0.06	360±50	0.59±0.08
GAK9	25	27	946	16.7	0.04	320±45	0.34±0.05
GAK15	31	27	807	30.1	0.10	232±32	0.29±0.04
KOD5	25	27	913	38.7	0.34	1039±145	1.14±0.16
KOD10	37	53	698	8.9	0.08	482±67	0.69±0.10
MID5	26	25	258	17.5	0.02	158±22	0.61±0.09
MID10	34	25	526	25.2	0.32	346±48	0.66±0.09
PWS2	22	80	240	58.3	0.17	172±24	0.72±0.10

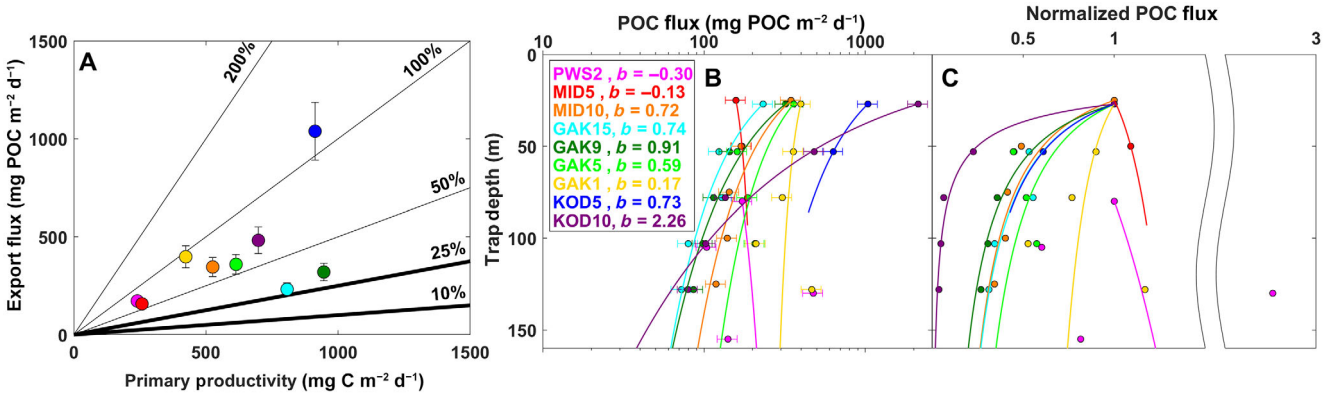

Fig. 3. Strength and efficiency of the biological carbon pump. (**A**) Chemically derived bulk **s**inking particulate organic carbon fluxes from drifting sediment traps vs. net primary productivity rates. Vertical error bars represent the average tube-to-tube standard deviation of about 14%. Diagonal lines show constant export ratios. Typical open ocean (10%) and typical shelf (25%) export ratio values are shown in bold (Dunne et al. 2007). (**B**) Chemically derived bulk sinking particulate organic carbon (POC) fluxes are shown over depth along with the best-fit attenuation curve and coefficient. Horizontal error bars represent the average tube-to-tube standard deviation of about 14%. (**C**) Normalized chemically derived sinking POC fluxes from drifting sediment traps over depth.

To put this in context, summertime POC export flux estimates at Ocean Station Papa were 9.5–78.2 mg C m^{-2} d^{-1} (Estapa et al. 2021) and 97 mg C m^{-2} d^{-1} (Buesseler and Boyd 2009), about one-fifth and one-third, respectively, of the average POC export flux in the Northern Gulf of Alaska. This difference is much larger than the expected collection bias between surface-tethered and neutrally buoyant sediment traps (Baker et al. 2020; Estapa et al. 2020). In the California Current Ecosystem, POC fluxes ranged from 42 to 437 mg C m^{-2} d^{-1} and averaged 185 ± 121 mg C m^{-2} d^{-1} (± 1 SD), with a median of 149 mg C m^{-2} d^{-1} (California Current Ecosystem LTER et al. 2022). Despite having similar or higher productivity, the average POC flux in the California Current Ecosystem was about half that of the Northern Gulf of Alaska. In addition, the maximum POC flux measured in the California Current Ecosystem was also about half of the highest POC export flux measured in the Northern Gulf of Alaska. This indicates stronger carbon export in the Northern Gulf of Alaska than at Ocean Station Papa and the California Current Ecosystem, perhaps due to larger or more aggregates forming or less remineralization. One explanation for why aggregates could be larger or more abundant is that the Northern Gulf of Alaska is known to have strong pycnoclines (Sarkar et al. 2005), which are associated with enhanced aggregation processes (MacIntyre et al. 1995; Prairie et al. 2013). *See* Supporting Information for a description of California Current Ecosystem data meta-analysis methods. Overall, we measured a strong biological carbon pump during the summer in the Northern Gulf of Alaska.

While we do not have previous carbon flux measurements from this region, high seasonal variability in carbon fluxes has been measured at Ocean Station Papa (Timothy et al. 2013). In addition, the Northern Gulf of Alaska is known to have high seasonal (Waite and Mueter 2013) and interannual (Strom et al. 2016) variability in chlorophyll and primary productivity. Therefore, high seasonal and interannual variability in POC flux is likely in the Northern Gulf of Alaska.

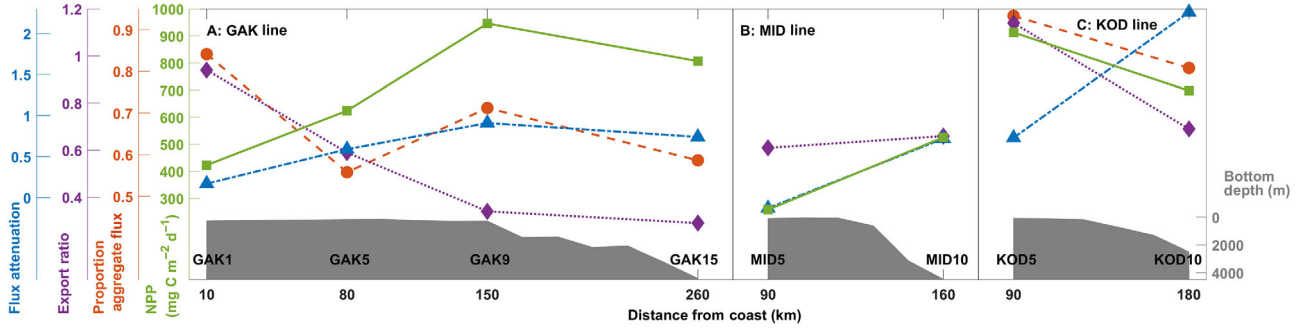

Fig. 4. Offshore gradient in biological carbon pump properties. Flux attenuation (blue triangles), export ratio (purple diamonds), proportion aggregate flux (orange circles), and net primary productivity (NPP; green squares) along with underlying bathymetry (filled gray patch) are plotted over distance from the coast for the (**A**) Gulf of Alaska (GAK) line, (**B**) Middle Island (MID) line, (**C**) Kodiak (KOD) line.

Efficiency of the biological carbon pump

The export ratio (i.e., export ratio = export flux/NPP, where export flux equals POC flux out of the euphotic zone) quantifies the efficiency of the biological carbon pump, with higher export ratios indicating a more efficient biological carbon pump. Export ratios ranged from 29% to 114% (average 67%, median 65%), indicating that POC was efficiently transported out of the euphotic zone during the summer of 2019 (Fig. 3A; Table 2). Stations with a high export ratio and relatively low primary productivity (e.g., GAK1 in yellow) can potentially indicate advected material entering the water column, non-steady-state conditions, or a collection bias. Export ratios tended to show a negative relationship with NPP and flux attenuation, being higher on the shelf and decreasing offshore (Fig. 4) and a positive relationship with export flux (Table 2). The MID line showed nearly identical export ratios at MID5 and MID10. We expect stations closer to the coast to exhibit more lateral advection of particles because the Alaska Coastal Current has a faster current speed than the Alaska Current (Reed and Schumacher 1986), and shallow shelves can allow for more resuspension of sediment from the seafloor. As such, resuspension and lateral advection of particles may cause decoupling between export flux and NPP and could result in higher export ratios, which we observed on the inner GAK and KOD lines (Fig. 4).

Overall, observed export ratios in the Northern Gulf of Alaska (67%) were very high compared to the average estimated export ratio in shelf ecosystems worldwide (~ 25%) (Dunne et al. 2007; Henson et al. 2015; Kelly et al. 2018). Global models predict export ratios of 0.1–0.15 for the Northern Gulf of Alaska (Henson et al. 2012), comparable to other measurements in the North Pacific. During summer, export ratios measured at Ocean Station Papa ranged from 6% to 18% and averaged 10% (Estapa et al. 2021) and were 14% in a previous study (Buesseler and Boyd 2009), about five times less than the average export ratio observed in the Northern Gulf of Alaska. This pattern is unexpected, as Ocean Station Papa and the Northern Gulf of Alaska share similar summertime nutrient limitation, rates of NPP, and phytoplankton community composition. However, the Northern Gulf of Alaska is closer to the coast and coastal areas generally are more associated with higher carbon flux and export efficiency (Dunne et al. 2007). In the California Current Ecosystem, a productive coastal upwelling system, summer export ratios ranged from 10% to 42% and averaged 30% ± 11% (± 1 SD), with a nearly identical median of 31% (*see* Supporting Information for how these values were calculated). The average export ratio in the California Current Ecosystem was about half of that in the Northern Gulf of Alaska despite the California Current Ecosystem being a high-productivity, high-flux site. Our data suggest that the summertime biological carbon pump in the Northern Gulf of Alaska is more efficient than previously assumed.

We expect that communities dominated by large cells will have higher export efficiency. Picophytoplankton and nanophytoplankton typically dominate the community during summertime, with 2019 as no exception (Cohen 2022). The proportion of Chl a > 20 μm (microphytoplankton) ranged from 0.04 at GAK9 to 0.34 at KOD5 and averaged 0.16, generally decreased with distance from shore, and did not correlate with NPP (Table 2). From these data, we do not know why GAK1, KOD5, and MID10 had the highest proportions of Chl a > 20 μm; however, generally, larger cells are often found in areas with more nutrient flux (Mousing et al. 2018). Perhaps higher iron availability near the coast allows for larger cells to grow, as diatoms are sensitive to iron limitation (Strom et al. 2016), or perhaps mesoscale eddies increased nutrient flux at some stations (Crawford et al. 2007). The proportion of Chl a > 20 μm positively correlated with export ratios (Pearson correlation coefficient, $r(7) = 0.49$, $p = 0.02$) (Fig. 5). This suggests that larger phytoplankton are driving carbon export efficiency, even though they make up a minority of total Chl a. Picophytoplankton and nanophytoplankton are thought to contribute to less efficient export due to their smaller size and lack of ballasting (Stokes 1851; Michaels and Silver 1988). However, other studies suggest that picophytoplankton can be exported efficiently if aggregates are formed (Richardson and Jackson 2007; Richardson 2019). Our data support the hypothesis that communities dominated by small cells can have efficient export, but more efficient export is likely when the proportion of large cells is higher.

POC fluxes generally decreased over depth consistent with a power-law curve (Fig. 3B,C), with an exponent (b) describing how efficiently POC is transported from the base of the euphotic zone into the deep ocean (e.g., originally proposed as $b = 0.86$) (Martin et al. 1987; Buesseler et al. 2007). In our

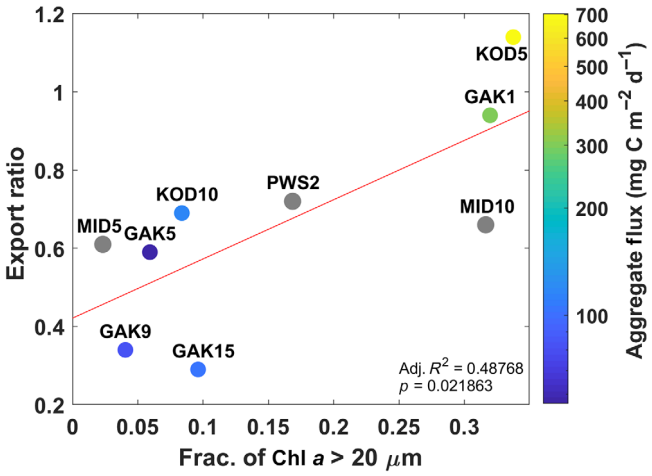

Fig. 5. Drivers of efficient export. Fraction of chlorophyll a (Chl a) > 20 μm significantly correlates with export ratio (Pearson correlation coefficient, $r(7) = 0.49$, $p = 0.02$) colored by aggregate flux (in mg C m^{-2} d^{-1}). Linear regression between the fraction of Chl a > 20 μm and export ratio is shown as the red line. Gray symbols indicate no associated aggregate flux measurement.

data, b ranged from −0.3 to 2.26, with lower values indicating a more efficient transfer of POC from the euphotic zone into the deep ocean. Our observations were lower (mean 0.63 ± 0.74, ± 1 SD, reference depth ∼ 25 m) than many typically observed (e.g., 0.86 in the northeast Pacific, reference depth 100 m (Martin et al. 1987), 1.16 at Ocean Station Papa, reference depth 100 m (Buesseler and Boyd 2009), 1.33 at station ALOHA, reference depth 150 m (Buesseler et al. 2007)). When interpreting these comparisons, it should be noted that flux attenuation is dependent on the depth of the upper trap (i.e., the reference depth) (Buesseler et al. 2020). It is somewhat unexpected that we measured such low POC flux attenuation in the Northern Gulf of Alaska, as higher flux areas, that is, coastal areas and higher latitude systems, often are modeled to have higher POC flux attenuation (Henson et al. 2012; Marsay et al. 2015). However, this topic is still being debated, as other modeling studies find a more efficient biological carbon pump in high-latitude systems (Weber et al. 2016). Our observed, rather than modeled, POC flux attenuation measurements provide important evidence of an efficient biological carbon pump in a subarctic coastal system.

POC flux attenuation also varied spatially in our study. PWS2 and MID5 both had negative attenuation coefficients, indicating an increase in carbon flux with depth. MID5 was the shallowest station (bottom depth ∼ 100 m) and, therefore, may have been experiencing resuspension from the seafloor or increased lateral transport due to the sharp gradient of bathymetry at nearby Middleton Island. The shallowest trap at PWS2 was 80 m, far below the actual euphotic zone depth of 22 m. This substantially increases the uncertainty of the best-fit b value. Overall, carbon flux attenuation increased with distance from shore along all lines and had a similar pattern as NPP (Fig. 4).

Contribution of carbon flux by particle types

To calculate the contribution of POC flux by particle type, we imaged the sinking particles, segmented those particles, identified particle types, and calculated particle volume by ESD. Finally, we modeled A and B values using Eq. 2 to find the best fit between the chemically derived POC flux and gel-estimated POC flux. Using this method, we can determine the contribution of each particle type (i.e., aggregates, fecal pellets, etc.) to the total POC flux.

The best-fit value A_{agg} for aggregates and unidentifiable particles was 1.5×10^{-10} mg C μm^{-3} with a 95% confidence interval of 0.7–2.2 $\times 10^{-10}$ mg C μm^{-3} (Supporting Information Table S2). The best-fit A_{FP} value for dense detritus, long, large loose, short, and mini fecal pellets was smaller than A_{agg} (1.2×10^{-11} mg C μm^{-3} with a 95% confidence interval of 0.1–3.8 $\times 10^{-11}$ mg C μm^{-3}). This smaller A value is paired with a larger B value of 1 (as compared to 0.8), such that aggregates and fecal pellets of the same ESD have carbon contents of the same order of magnitude over the size range we analyze from the polyacrylamide gels (∼ 20–3000 μm). These values agree well with previous empirically derived or model-derived values. *See* Supporting Information for a mini-review of these model results compared to empirical values (Supporting Information Text S1; Supporting Information Fig. S4; Supporting Information Table S4).

The majority of the POC flux at nearly all stations and depths comes from aggregates, ranging from 41% to 93% and averaging 61% ± 13% (± 1 SD) (Fig. 6; Supporting Information Table S5). This majority further increases when considering all non-fecal pellet sources, that is, the combined contribution of aggregates, dense detritus, and unidentifiable particles, ranging from 54% to 96% and averaging 74% ± 11% (± 1 SD). Most particles identified as aggregates and dense detritus appeared to be made up largely of green phytoplankton-derived material. Carbon from fecal pellets made up a small percentage of sinking carbon flux, ranging from 4% to 45% and averaging 25% ± 10% (± 1 SD). Both overall and relative carbon flux from short fecal pellets, likely coming from small copepods (e.g., *Pseudocalanus*) or larvaceans (Wilson et al. 2008), increased with distance from shore. Long fecal pellets, likely from large copepods (e.g., *Calanus marshallae*, *Metridia pacifica*) or euphausiids (Wilson et al. 2008), were the most important fecal pellet type for carbon flux and relative carbon flux at all stations except KOD5 where large loose pellets, mini pellets, and short pellets all contributed higher carbon flux and relative flux than long fecal pellets. Ninety-five percent of the variability in overall gel-derived carbon flux was due to variability in aggregate carbon flux. The relative contribution of aggregates decreased offshore on the KOD line and decreased offshore on the GAK line with some variability (Fig. 4). Aggregates contributed the most to carbon flux at GAK1, followed by GAK9, GAK15, and GAK5. This indicates that grazing pressure from fecal pellet-producing zooplankton could be relatively higher offshore. Trends in total fecal pellet carbon flux were mostly due to relative and total contributions of short fecal pellets. Therefore, we looked at the distributions of two taxa that produce short fecal pellets: small copepods (e.g., *Pseudocalanus*) and larvaceans. *Pseudocalanus* have been observed to be in higher abundance on the shelf during summer in the Northern Gulf of Alaska, so they are unlikely to contribute to the pattern we see of increasing flux of short fecal pellets offshore (Napp et al. 2005). Certain species of grazing larvaceans (e.g., *Fritillaria borealis*) have been observed to be in higher abundance offshore during the summer in this region (Doubleday and Hopcroft 2015) and could potentially explain the pattern of short fecal pellets. Another explanation is that the pycnocline is stronger near the coast, which is associated with enhanced aggregation (MacIntyre et al. 1995; Prairie et al. 2013). Coastal stations with the highest export efficiency also had higher proportions of Chl $a > 20$ μm (Fig. 5); these patterns may be driven by larger phytoplankton, such as diatoms in poor physiological conditions due to macronutrient limitation, that are known to sink rapidly (Michaels and Silver 1988). These results are in line with previous observations of marine particles in the Northern Gulf of Alaska, where most large particles (> 0.5 mm) were

observed to be detrital aggregates (Turner et al. 2017). However, at Ocean Station Papa during the summer, long, mini, and salp fecal pellets have been observed to dominate carbon flux at all depths (~ 100–500 m) (Durkin et al. 2021). Overall, we observed an efficient biological carbon pump with high export ratios and a predominance of aggregate flux.

GAK1, GAK5, and GAK9 showed some signs of increasing gel-derived POC flux over depth, while the chemically derived POC fluxes decreased with depth at these stations (Fig. 6). This could be explained by carbon-to-volume ratios that change with depth. As particles sink and undergo remineralization, their mass may decrease while their ESD remains the same. Future studies should explore this idea to determine whether improving the fit between chemically-derived and gel-derived POC fluxes is possible. In addition, we are most likely to miss small particles when identifying particles in the gel images, therefore underestimating carbon flux from small particles. The mismatch between chemically derived and gel-derived carbon flux could also further support the theory that small particles are important to carbon flux (Richardson and Jackson 2007; Durkin et al. 2015; Richardson 2019).

Drivers of carbon export

To determine if certain particle types were correlated with higher carbon export, a PCA was performed on the carbon flux by particle type at each station/depth sample (Fig. 7A). Aggregate carbon flux is strongly associated with total carbon flux, phytoplankton flux, and long fecal pellet flux (Fig. 7B). Gel-estimated carbon flux tended to decrease as stations moved offshore (Fig. 7C). Total number concentration (i.e., ambient particle concentrations) and total number flux are both positively correlated to carbon flux. Interestingly, sinking velocity, mean sinking particle size, and trap depth are poor indicators of total carbon flux. The carbon-to-volume ratio has an inverse relationship with carbon flux. Estimated carbon flux from aggregates, long fecal pellets, and phytoplankton are significantly correlated (linear regression, F-statistic, $p < 0.05$) with the total carbon flux; however, carbon flux from aggregates most strongly correlates with carbon flux.

Efficient export in the Northern Gulf of Alaska during summer is driven by a few parameters. Export ratio correlated significantly with the proportion of Chl a $> 20\,\mu$m, total aggregate flux, export flux, and percent aggregate flux (Pearson, $p \leq 0.05$) (Fig. 5). Aggregate flux also significantly correlated with the proportion of Chl a $> 20\,\mu$m (Pearson, $p \leq 0.05$) (Fig. 5). Interestingly, NPP does not significantly correlate with any other variable. KOD5 and GAK1, for example, had the highest export ratios, proportion of Chl a $> 20\,\mu$m, and contributions of aggregate flux. This provides a framework for conditions that allow for efficient export, besides efficient export driven by high fecal pellet flux as previously described (Ebersbach and Trull 2008; Laurenceau-Cornec et al. 2015).

To determine if certain particle types more efficiently transport carbon to depth, we performed linear regressions on carbon flux over depth from different stations and different particle types (Supporting Information Fig. S5). Certain particle types are not more likely to reach different depths than others. Only four of these carbon fluxes by station and particle type combinations have significant relationships over depth; at GAK15, aggregates decreased over depth with a slope of -0.67 ($p = 0.025$), dense detritus decreased over depth with a slope of -0.04 ($p = 0.005$), and short fecal pellets decreased over depth with a slope of -0.23 ($p = 0.016$); at GAK9 large loose fecal pellets increased over depth with a slope of 0.10 ($p = 0.011$). Within each particle type, the slopes also have mixed positive and negative relationships depending on the station. Therefore, these data do not strongly support a claim that carbon from certain particle types is more or less likely to reach deeper depths than other particle types.

Debate continues over whether zooplankton fecal pellet production through the consumption of phytoplankton and aggregates results in higher or lower carbon export (Turner 2015). In some studies, systems with less dense, sometimes smaller material that is repackaged into larger, denser fecal pellets result in higher carbon export (Iversen and Lampitt 2020). In other studies, mineral ballasted aggregates exported carbon more effectively than fecal pellets (Armstrong et al. 2002), as fecal pellets can have high rates of particle-associated microbial respiration (Smetacek 1985; Ploug et al. 2008*a*; Kobari et al. 2013). Our results suggest that particle type did not strongly impact the efficiency at which POC was transferred from the euphotic zone to the deep ocean during summer in the Northern Gulf of Alaska. One caveat is that our deepest trap was around 125 m, relatively shallow. It is possible that the particle type-specific effects only apply to the deeper ocean.

Performing a similar analysis against particle sizes, we found no significant difference in ESDs with depth, station, or type (Supporting Information Fig. S6). The absence of relationships between particle size and depth is consistent with three different explanations. First, if particle formation below the euphotic zone is minor compared to flux from the euphotic zone, then consistency of particle sizes would imply similar attenuation length scales across particle classes. Second, if particle formation below the euphotic zone is significant relative to euphotic zone export, then it implies that particles formed in the twilight zone have size spectra similar to those formed in the euphotic zone, and perhaps that similar repackaging processes are dominant. Third, it is possible that the particle size-specific effects are relatively slow compared to the residence time of sinking particles above our traps and that deeper traps may resolve such patterns.

Marine heatwave

During 2019 sea surface temperatures in the Northern Gulf of Alaska were about 2°C warmer than the long-term mean (Danielson et al. 2022), characteristic of a marine heatwave. The 2019 marine heatwave was associated with higher

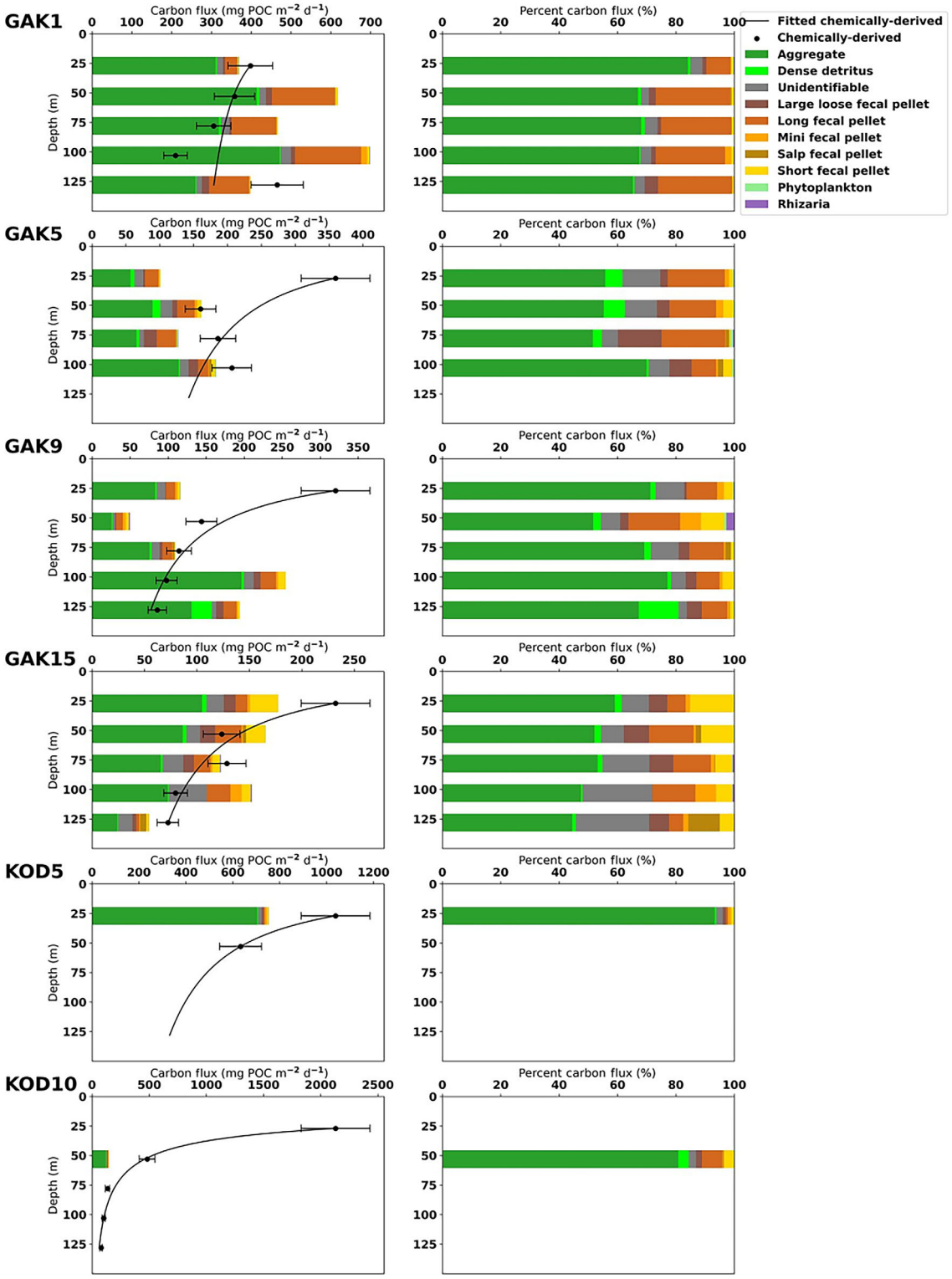

Fig. 6. Contribution of carbon flux by particle type. Left columns: Depth profiles of gel-derived particulate organic carbon (POC) flux from June and July 2019 in the Northern Gulf of Alaska by each particle type at the indicated locations. Black circles show the corresponding chemically derived bulk POC fluxes with POC attenuation shown in black. Horizontal error bars indicate an average tube-to-tube error of about 14%. Right columns: Depth profiles of relative POC flux by particle type from gel analysis.

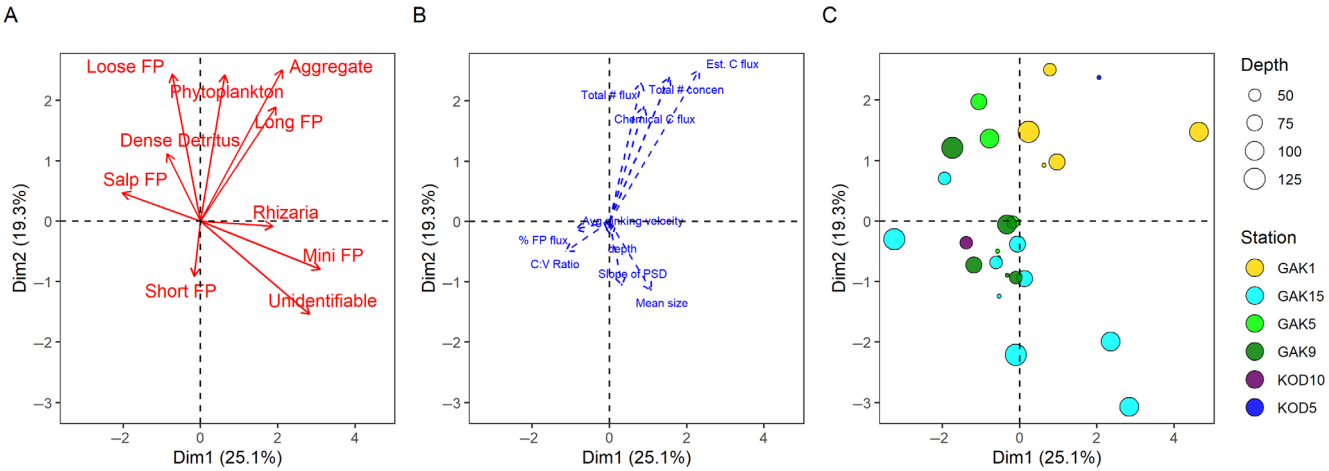

Fig. 7. (**A**) PCA on the carbon flux by particle type at each station/depth location, shown in red arrows: FP, fecal pellet. (**B**) Quantitative supplementary variables estimated at each depth/station pair: total gel-estimated carbon flux (Est. C flux), total chemically derived particulate organic carbon flux (Chemical C flux), total number concentration averaged from the 50 m above the trap depth (Total # concen), gel-derived total number flux (Total # flux), average sinking velocity (Avg. sinking velocity), relative contribution of fecal pellets to carbon flux (% FP flux), calculated carbon to volume ratio (C : V ratio), slope of the gel-derived particle size distribution of sinking particles (slope of PSD), depth of the trap (depth), and average sinking particle size (mean size). (**C**) Individuals are plotted as colored dots corresponding to a sample (i.e., one depth/station pair). Colors and size correspond with the station and depth at which the sediment trap sampled, respectively.

abundances of picophytoplankton observed during the summer in the Northern Gulf of Alaska (Cohen 2022). Generally, warmer ocean temperatures are thought to increase microbial respiration rates and decrease the sinking speed of particles generated by the food web (Michaels and Silver 1988; Vaqué et al. 2019). However, we measured a strong and efficient biological carbon pump characterized by a high proportion of aggregate flux during the summer in the Northern Gulf of Alaska. If our observations of a strong and efficient biological carbon pump are representative of this system, this might imply that biological carbon pump in the Northern Gulf of Alaska is even stronger and more efficient in non-heatwave summers.

Conclusions

This study is the first description of the biological carbon pump in the Northern Gulf of Alaska. The biological carbon pump was strong and efficient during the summer of 2019. NPP was typical of other past measurements in the subarctic and coastal North Pacific; however, POC fluxes and export ratios were much higher, with lower carbon flux attenuation and higher contributions of aggregates, than prior results from similar regions (Buesseler and Boyd 2009; Durkin et al. 2021; Estapa et al. 2021). By using a comprehensive approach that brings together sediment trap sampling and imaging, optically measured distribution of sinking and suspended particles, and incubations, our data suggest that the main driver of carbon flux in the Northern Gulf of Alaska during summer was aggregation processes and the main drivers of efficient carbon export were the proportion of Chl *a* in the large size fraction (> 20 μm) and aggregation processes. These results lead us to question our expectations about conditions and processes creating strong and efficient flux events. Clearly strong and efficient flux events can originate from communities dominated by picophytoplankton and nanophytoplankton, with moderate contribution from zooplankton fecal pellets. These results can help improve the climate and ecological models for this region and the broader subarctic coastal region to better predict the fate of organic material produced through photosynthesis.

Data availability statement

All data associated with this study are publicly available in the Supporting Information and on GitHub (https://github.com/shodaly2/ODaly_et_al_2023_L_and_O_NGA_Flux).

References

Aguilar-Islas, A. M., M. J. M. Séguret, R. Rember, K. N. Buck, P. Proctor, C. W. Mordy, and N. B. Kachel. 2016. Temporal variability of reactive iron over the Gulf of Alaska shelf. Deep-Sea Res. II: Top. Stud. Oceanogr. **132**: 90–106. doi:10.1016/j.dsr2.2015.05.004

Alldredge, A. 1998. The carbon, nitrogen and mass content of marine snow as a function of aggregate size. Deep-Sea Res. I: Oceanogr. Res. Pap. **45**: 529–541. doi:10.1016/S0967-0637(97)00048-4

Armstrong, R., C. Lee, J. Hedges, S. Honjo, and S. G. Wakeham. 2002. A new, mechanistic model for organic carbon fluxes in the ocean based on the quantitative association of POC with ballast minerals. Deep-Sea Res. I:

Oceanogr. Res. Pap. **49**: 219–236. doi:10.1016/S0967-0645(01)00101-1

Baker, C. A., M. L. Estapa, M. Iversen, R. Lampitt, and K. Buesseler. 2020. Are all sediment traps created equal? An intercomparison study of carbon export methodologies at the PAP-SO site. Prog. Oceanogr. **184**: 102317. doi:10.1016/j.pocean.2020.102317

Bernstein, R. E., P. R. Betzer, R. A. Feely, R. H. Byrne, M. F. Lamb, and A. F. Michaels. 1987. Acantharian fluxes and strontium to chlorinity ratios in the North Pacific Ocean. Science **237**: 1490–1494. doi:10.1126/science.237.4821.1490

Bishop, J. K. B., R. W. Collier, D. R. Kettens, and J. M. Edmond. 1980. The chemistry, biology, and vertical flux of particulate matter from the upper 1500 m of the Panama Basin. Deep-Sea Res. I: Oceanogr. Res. Pap. **27**: 615–640. doi:10.1016/0198-0149(80)90077-1

Bishop, J. K., J. C. Stepien, and P. H. Wiebe. 1986. Particulate matter distributions, chemistry and flux in the Panama Basin: Response to environmental forcing. Prog. Oceanogr. **17**: 1–59. doi:10.1016/0079-6611(86)90024-8

Booth, B. C., J. Lewin, and S. R. Postel. 1993. Temporal variation in the structure of autotrophic and heterotrophic communities in the subarctic Pacific. Prog. Oceanogr. **32**: 57–99. doi:10.1016/0079-6611(93)90009-3

Buesseler, K. O., and P. W. Boyd. 2009. Shedding light on processes that control particle export and flux attenuation in the twilight zone of the open ocean. Limnol. Oceanogr. **54**: 1210–1232. doi:10.4319/lo.2009.54.4.1210

Buesseler, K. O., P. W. Boyd, E. E. Black, and D. A. Siegel. 2020. Metrics that matter for assessing the ocean biological carbon pump. Proc. Natl. Acad. Sci. USA **117**: 9679–9687. doi:10.1073/pnas.1918114117

Buesseler, K. O., and others. 2007. Revisiting carbon flux through the ocean's twilight zone. Science **316**: 567–570. doi:10.1126/science.1137959

California Current Ecosystem LTER, and G. Goericke. 2022. Water column primary production per day integrated over the euphotic zone from CCE LTER process cruises in the California Current System, 2006–2019 (ongoing). ver 5. Environmental Data Initiative. doi:10.6073/pasta/9dddc0e6ab3c0ac48d41e04811a1870f

California Current Ecosystem LTER, M. Stukel, and M. Landry. 2022. Exported particulate carbon and nitrogen measurements from 4-day sediment trap deployments in the CCE region, 2007–2019 (ongoing). ver 7. Environmental Data Initiative. doi:10.6073/pasta/cdee03ef7b17c2a4027a4a8b33c5b09b

Childers, A. R., T. E. Whitledge, and D. A. Stockwell. 2005. Seasonal and interannual variability in the distribution of nutrients and chlorophyll *a* across the Gulf of Alaska shelf: 1998-2000. Deep-Sea Res. II: Top. Stud. Oceanogr. **52**: 193–216. doi:10.1016/j.dsr2.2004.09.018

Cohen, J. 2022. Shifts in microbial community composition during the 2019 Pacific marine heatwave in the northern Gulf of Alaska. MS Thesis. Univ. of Alaska Fairbanks.

Crawford, W. R., P. J. Brickley, and A. C. Thomas. 2007. Mesoscale eddies dominate surface phytoplankton in Northern Gulf of Alaska. Prog. Oceanogr. **75**: 287–303. doi:10.1016/j.pocean.2007.08.016

Danielson, S. L., T. D. Hennon, D. H. Monson, R. M. Suryan, R. W. Campbell, S. J. Baird, K. Holderied, and T. J. Weingartner. 2022. Temperature variations in the northern Gulf of Alaska across synoptic to century-long time scales. Deep-Sea Res. II Top. Stud. Oceanogr. **203**: 105155. doi:10.1016/j.dsr2.2022.105155

De La Rocha, C. L., and U. Passow. 2007. Factors influencing the sinking of POC and the efficiency of the biological carbon pump. Deep-Sea Res. II: Top. Stud. Oceanogr. **54**: 639–658. doi:10.1016/j.dsr2.2007.01.004

Doubleday, A. J., and R. R. Hopcroft. 2015. Interannual patterns during spring and late summer of larvaceans and pteropods in the coastal Gulf of Alaska, and their relationship to pink salmon survival. J. Plankton Res. **37**: 134–150. doi:10.1093/plankt/fbu092

Dunne, J. P., J. L. Sarmiento, and A. Gnanadesikan. 2007. A synthesis of global particle export from the surface ocean and cycling through the ocean interior and on the seafloor. Glob. Biogeochem. Cycles **21**: 1–16. doi:10.1029/2006GB002907

Durkin, C. A., M. L. Estapa, and K. O. Buesseler. 2015. Observations of carbon export by small sinking particles in the upper mesopelagic. Mar. Chem. **175**: 72–81. doi:10.1016/j.marchem.2015.02.011

Durkin, C. A., K. O. Buesseler, I. Cetinić, M. L. Estapa, R. P. Kelly, and M. Omand. 2021. A visual tour of carbon export by sinking particles. Glob. Biogeochem. Cycles **35**: e2021GB006985. doi:10.1029/2021GB006985

Ebersbach, F., and T. Trull. 2008. Sinking particle properties from polyacrylamide gels during the KErguelen Ocean and Plateau compared Study (KEOPS): Zooplankton control of carbon export in an area of persistent natural iron inputs in the Southern Ocean. Limnol. Oceanogr. **53**: 212–224. doi:10.4319/lo.2008.53.1.0212

Estapa, M., J. Valdes, K. Tradd, J. Sugar, M. Omand, and K. Buesseler. 2020. The neutrally buoyant sediment trap: Two decades of progress. J. Atmos. Ocean. Technol. **37**: 957–973. doi:10.1175/JTECH-D-19-0118.1

Estapa, M., and others. 2021. Biogenic sinking particle fluxes and sediment trap collection efficiency at Ocean Station Papa. Elementa **9**: 00122. doi:10.1525/elementa.2020.00122

Guidi, L., G. A. Jackson, L. Stemmann, J. C. Miquel, M. Picheral, and G. Gorsky. 2008. Relationship between particle size distribution and flux in the mesopelagic zone. Deep-Sea Res. I: Oceanogr. Res. Pap. **55**: 1364–1374. doi:10.1016/j.dsr.2008.05.014

Hama, T., T. Miyazaki, Y. Ogawa, T. Iwakuma, M. Takahashi, A. Otsuki, and S. Ichimura. 1983. Measurement of photosynthetic production of a marine phytoplankton population using a stable ^{13}C isotope. Mar. Biol. **73**: 31–36. doi:10.1007/BF00396282

Henson, S. A., R. Sanders, E. Madsen, P. J. Morris, F. Le Moigne, and G. D. Quartly. 2011. A reduced estimate of the strength of the ocean's biological carbon pump. Geophys. Res. Lett. **38**: 1–5. doi:10.1029/2011GL046735

Henson, S. A., R. Sanders, and E. Madsen. 2012. Global patterns in efficiency of particulate organic carbon export and transfer to the deep ocean. Glob. Biogeochem. Cycles **26**: 1–14. doi:10.1029/2011GB004099

Henson, S. A., A. Yool, and R. Sanders. 2015. Variability in efficiency of particulate organic carbon export: A model study. Glob. Biogeochem. Cycles **29**: 33–45. doi:10.1002/2014GB004965

Iversen, M. H., and H. Ploug. 2010. Ballast minerals and the sinking carbon flux in the ocean: Carbon-specific respiration rates and sinking velocity of marine snow aggregates. Biogeosciences **7**: 2613–2624. doi:10.5194/bg-7-2613-2010

Iversen, M. H., E. A. Pakhomov, B. P. V. Hunt, H. van der Jagt, D. Wolf-Gladrow, and C. Klaas. 2017. Sinkers or floaters? Contribution from salp pellets to the export flux during a large bloom event in the Southern Ocean. Deep-Sea Res. II: Top. Stud. Oceanogr. **138**: 116–125. doi:10.1016/j.dsr2.2016.12.004

Iversen, M. H., and R. S. Lampitt. 2020. Size does not matter after all: No evidence for a size-sinking relationship for marine snow. Prog. Oceanogr. **189**: 102445. doi:10.1016/j.pocean.2020.102445

Jaeger, J. M., and C. A. Nittrouer. 2006. A quantitative examination of modern sedimentary lithofacies formation on the glacially influenced Gulf of Alaska continental shelf. Cont. Shelf Res. **26**: 2178–2204. doi:10.1016/j.csr.2006.07.014

Johnson, C. P., X. Li, and B. E. Logan. 1996. Settling velocities of fractal aggregates. Environ. Sci. Technol. **30**: 1911–1918. doi:10.1021/es950604g

Kelly, T. B., R. Goericke, M. Kahru, H. Song, and M. R. Stukel. 2018. CCE II: Spatial and interannual variability in export efficiency and the biological pump in an eastern boundary current upwelling system with substantial lateral advection. Deep-Sea Res. I: Oceanogr. Res. Pap. **140**: 14–25. doi:10.1016/j.dsr.2018.08.007

Knauer, G. A., J. H. Martin, and K. W. Bruland. 1979. Fluxes of particulate carbon, nitrogen, and phosphorus in the upper water column of the northeast Pacific. Deep-Sea Res. I: Oceanogr. Res. Pap. **26**: 97–108. doi:10.1016/0198-0149(79)90089-X

Kobari, T., M. Kitamura, and others. 2013. Impacts of the wintertime mesozooplankton community to downward carbon flux in the subarctic and subtropical Pacific Oceans. Deep-Sea Res. I: Oceanogr. Res. Pap. **81**: 78–88. doi:10.1016/j.dsr.2013.07.003

Ladd, C., W. Cheng, and S. Salo. 2016. Gap winds and their effects on regional oceanography part II: Kodiak Island, Alaska. Deep-Sea Res. II: Top. Stud. Oceanogr. **132**: 54–67. doi:10.1016/j.dsr2.2015.08.005

Lampitt, R. S., I. Salter, and D. Johns. 2009. Radiolaria: Major exporters of organic carbon to the deep ocean. Glob. Biogeochem. Cycles **23**: 1–9. doi:10.1029/2008GB003221

Laufkötter, C., and others. 2016. Projected decreases in future marine export production: The role of the carbon flux through the upper ocean ecosystem. Biogeosciences **13**: 4023–4047. doi:10.5194/bg-13-4023-2016

Laurenceau-Cornec, E. C., and others. 2015. The relative importance of phytoplankton aggregates and zooplankton fecal pellets to carbon export: Insights from free-drifting sediment trap deployments in naturally iron-fertilised waters near the Kerguelen Plateau. Biogeosciences **12**: 1007–1027. doi:10.5194/bg-12-1007-2015

MacIntyre, S., A. L. Alldredge, and C. C. Gotschalk. 1995. Accumulation of marines now at density discontinuities in the water column. Limnol. Oceanogr. **40**: 449–468. doi:10.4319/lo.1995.40.3.0449

Macklin, S. A., N. A. Bond, and J. P. Walker. 1990. Structure of a low-level jet over lower Cook Inlet, Alaska. Mon. Weather Rev. **118**: 2568–2578. doi:10.1175/1520-0493(1990)118<2568:SOALLJ>2.0.CO;2

Marsay, C. M., E. P. Achterberg, K. Pabortsava, S. A. Henson, R. J. Sanders, and R. S. Lampitt. 2015. Attenuation of sinking particulate organic carbon flux through the mesopelagic ocean. Proc Natl Acad Sci USA **112**: 1089–1094. doi:10.1073/pnas.1415311112

Martin, J. H., G. A. Knauer, D. M. Karl, and W. W. Broenkow. 1987. VERTEX: Carbon cycling in the northeast Pacific. Deep-Sea Res. I: Oceanogr. Res. Pap. **34**: 267–285. doi:10.1016/0198-0149(87)90086-0

Menden-Deuer, S., and E. J. Lessard. 2000. Carbon to volume relationships for dinoflagellates, diatoms, and other protist plankton. Limnol. Oceanogr. **45**: 569–579. doi:10.4319/lo.2000.45.3.0569

Michaels, A. F., and M. W. Silver. 1988. Primary production, sinking fluxes and the microbial food web. Deep-Sea Res. I: Oceanogr. Res. Pap. **35**: 473–490. doi:10.1016/0198-0149(88)90126-4

Michaels, A. F., D. A. Caron, N. R. Swanberg, F. A. Howse, and C. M. Michaels. 1995. Planktonic sarcodines (Acantharia, Radiolaria, Foraminifera) in surface waters near Bermuda: Abundance, biomass and vertical flux. J. Plankton Res. **17**: 131–163. doi:10.1093/plankt/17.1.131

Moran, S. B., R. P. Kelly, K. Iken, J. T. Mathis, M. W. Lomas, and R. Gradinger. 2012. Seasonal succession of net primary productivity, particulate organic carbon export, and autotrophic community composition in the eastern Bering Sea. Deep-Sea Res. II: Top. Stud. Oceanogr. **65–70**: 84–97. doi:10.1016/j.dsr2.2012.02.011

Mordy, C. W., and others. 2019. Patterns of flow in the canyons of the northern Gulf of Alaska. Deep-Sea Res. II: Top. Stud. Oceanogr. **165**: 203–220. doi:10.1016/j.dsr2.2019.03.009

Moriarty, R., E. T. Buitenhuis, and C. Le Quéré. 2013. Distribution of known macrozooplankton abundance and biomass in the global ocean. Earth Syst. Sci. Data **5**: 241–257. doi:10.5194/essd-5-241-2013

Mousing, E. A., K. Richardson, and M. Ellegaard. 2018. Global patterns in phytoplankton biomass and community size structure in relation to macronutrients in the open ocean. Limnol. Oceanogr. **63**: 1298–1312. doi:10.1002/lno.10772

Muench, R. D., H. O. Mofjeld, and R. L. Charnell. 1978. Oceanographic conditions in lower cook inlet: Spring and summer 1973. J. Geophys. Res. **83**: 5090–5098. doi:10.1029/jc083ic10p05090

Napp, J. M., L. S. Incze, P. B. Ortner, D. L. W. Siefert, and L. Britt. 1996. The plankton of Shelikof Strait, Alaska: Standing stock, production, mesoscale variability and their relevance to larval fish survival. Fish. Oceanogr. **5**: 19–38. doi:10.1111/j.1365-2419.1996.tb00080.x

Napp, J. M., R. R. Hopcroft, C. T. Baier, and C. Clarke. 2005. Distribution and species-specific egg production of *Pseudocalanus* in the Gulf of Alaska. J. Plankton Res. **27**: 415–426. doi:10.1093/plankt/fbi015

O'Daly, S. H., S. L. Danielson, S. M. Hardy, R. R. Hopcroft, C. Lalande, D. A. Stockwell, and A. M. P. McDonnell. 2020. Extraordinary carbon fluxes on the shallow Pacific Arctic shelf during a remarkably warm and Low Sea ice period. Front. Mar. Sci. **7**: 548931. doi:10.3389/fmars.2020.548931

Owens, S. A., K. O. Buesseler, C. H. Lamborg, J. Valdes, M. W. Lomas, R. J. Johnson, D. K. Steinberg, and D. A. Siegel. 2013. A new time series of particle export from neutrally buoyant sediments traps at the Bermuda Atlantic Time-series Study site. Deep-Sea Res. I: Oceanogr. Res. Pap. **72**: 34–47. doi:10.1016/j.dsr.2012.10.011

Parsons, T. R. 1987. Ecological relations, p. 561–570. *In* D. W. Hood and S. T. Zimmerman [eds.], The Gulf of Alaska: Physical environment and biological resources. NOAA, U.S. Department of Commerce.

Ploug, H., M. H. Iversen, and G. Fischer. 2008*a*. Ballast, sinking velocity, and apparent diffusivity within marine snow and zooplankton fecal pellets: Implications for substrate turnover by attached bacteria. Limnol. Oceanogr. **53**: 1878–1886. doi:10.4319/lo.2008.53.5.1878

Ploug, H., M. H. Iversen, M. Koski, and E. T. Buitenhuis. 2008*b*. Production, oxygen respiration rates, and sinking velocity of copepod fecal pellets: Direct measurements of ballasting by opal and calcite. Limnol. Oceanogr. **53**: 469–476. doi:10.4319/lo.2008.53.2.0469

Prairie, J., and others. 2013. Delayed settling of marine snow at sharp density transitions driven by fluid entrainment and diffusion-limited retention. Mar. Ecol. Prog. Ser. **487**: 185–200. doi:10.3354/meps10387

Reed, R. K., and J. D. Schumacher. 1986. Physical oceanography. *In* D. W. Hood and S. T. Zimmerman [eds.], The Gulf of Alaska: Physical environment and biological resources. NOAA, U.S. Department of Commerce.

Richardson, T. L. 2019. Mechanisms and pathways of small-phytoplankton export from the surface ocean. Ann. Rev. Mar. Sci. **11**: 57–74. doi:10.1146/annurev-marine-121916-063627

Richardson, T. L., and G. A. Jackson. 2007. Small phytoplankton and carbon export from the Surface Ocean. Science **315**: 838–840. doi:10.1126/science.1133471

Royer, T. C., and W. J. Emery. 1987. Circulation in the Gulf of Alaska, 1981. Deep-Sea Res. I: Oceanogr. Res. Pap. **34**: 1361–1377. doi:10.1016/0198-0149(87)90132-4

Sambrotto, R. N., and C. Lorenzen. 1987. Phytoplankton and primary production, p. 249–282. *In* D. W. Hood and T. S. Zimmerman [eds.], The Gulf of Alaska, physical environmental and biological resources. NOAA, U.S. Department of Commerce.

Sarkar, N., T. C. Royer, and C. E. Grosch. 2005. Hydrographic and mixed layer depth variability on the shelf in the northern Gulf of Alaska, 1974-1998. Cont. Shelf Res. **25**: 2147–2162. doi:10.1016/j.csr.2005.07.006

Siegel, D. A., K. O. Buesseler, S. C. Doney, S. F. Sailley, M. J. Behrenfeld, and P. W. Boyd. 2014. Global assessment of ocean carbon export by combining satellite observations and food-web models. Glob. Biogeochem. Cycles **28**: 181–196. doi:10.1002/2013GB004743

Silver, M. W., and K. W. Bruland. 1981. Differential feeding and fecal pellet composition of salps and pteropods, and the possible origin of the deep-water flora and olive-green "cells". Mar. Biol. **62**: 263–273. doi:10.1007/BF00397693

Smetacek, V. S. 1985. Role of sinking in diatom life-history cycles: Ecological, evolutionary and geological significance. Mar. Biol. **84**: 239–251. doi:10.1007/BF00392493

Stabeno, P. J., N. A. Bond, A. J. Hermann, N. B. Kachel, C. W. Mordy, and J. E. Overland. 2004. Meteorology and oceanography of the northern Gulf of Alaska. Cont. Shelf Res. **24**: 859–897. doi:10.1016/j.csr.2004.02.007

Stemmann, L., G. A. Jackson, and G. Gorsky. 2004. A vertical model of particle size distributions and fluxes in the midwater column that includes biological and physical processes—Part II: Application to a three year survey in the NW Mediterranean Sea. Deep-Sea Res. I: Oceanogr. Res. Pap. **51**: 885–908. doi:10.1016/j.dsr.2004.03.002

Stokes, G. G. 1851. On the effect of the internal friction of fluids on the motion of pendulums. Trans. Cambridge Philos. Soc. **9**: 8–106.

Strom, S. L., M. A. Brainard, J. L. Holmes, and M. B. Olson. 2001. Phytoplankton blooms are strongly impacted by microzooplankton grazing in coastal North Pacific waters. Mar. Biol. **138**: 355–368. doi:10.1007/s002270000461

Strom, S. L., M. B. Olson, E. L. Macri, and C. W. Mordy. 2006. Cross-shelf gradients in phytoplankton community

structure, nutrient utilization, and growth rate in the coastal Gulf of Alaska. Mar. Ecol. Prog. Ser. **328**: 75–92. doi:10.3354/meps328075

Strom, S. L., E. L. Macri, and M. B. Olson. 2007. Microzooplankton grazing in the coastal Gulf of Alaska: Variations in top-down control of phytoplankton. Limnol. Oceanogr. **52**: 1480–1494. doi:10.4319/lo.2007.52.4.1480

Strom, S. L., K. A. Fredrickson, and K. J. Bright. 2016. Spring phytoplankton in the eastern coastal Gulf of Alaska: Photosynthesis and production during high and low bloom years. Deep-Sea Res. II: Top. Stud. Oceanogr. **132**: 107–121. doi:10.1016/j.dsr2.2015.05.003

Strom, S., and K. Fredrickson. 2020. Primary productivity estimates from NGA-LTER research cruises in the Gulf of Alaska, 2018-2020. Research Workspace. doi:10.24431/rw1k45b

Stukel, M. R., H. Song, R. Goericke, and A. J. Miller. 2018. The role of subduction and gravitational sinking in particle export, carbon sequestration, and the remineralization length scale in the California Current Ecosystem. Limnol. Oceanogr. **63**: 363–383. doi:10.1002/lno.10636

Timothy, D. A., C. S. Wong, J. E. Barwell-Clarke, J. S. Page, L. A. White, and R. W. Macdonald. 2013. Climatology of sediment flux and composition in the subarctic Northeast Pacific Ocean with biogeochemical implications. Prog. Oceanogr. **116**: 95–129. doi:10.1016/j.pocean.2013.06.017

Turner, J. T. 2015. Zooplankton fecal pellets, marine snow, phytodetritus and the ocean's biological pump. Prog. Oceanogr. **130**: 205–248. doi:10.1016/j.pocean.2014.08.005

Turner, J. S., J. L. Pretty, and A. M. P. McDonnell. 2017. Marine particles in the Gulf of Alaska shelf system: Spatial patterns and size distributions from in situ optics. Cont. Shelf Res. **145**: 13–20. doi:10.1016/j.csr.2017.07.002

van Oevelen, D., K. van den Meersche, F. J. R. Meysman, K. Soetaert, J. J. Middelburg, and A. F. Vézina. 2010. Quantifying food web flows using linear inverse models. Ecosystems **13**: 32–45. doi:10.1007/s10021-009-9297-6

Vaqué, D., and others. 2019. Warming and CO_2 enhance Arctic heterotrophic microbial activity. Front. Microbiol. **10**: 494. doi:10.3389/fmicb.2019.00494

Waite, J. N., and F. J. Mueter. 2013. Spatial and temporal variability of chlorophyll-*a* concentrations in the coastal Gulf of Alaska, 1998-2011, using cloud-free reconstructions of SeaWiFS and MODIS-Aqua data. Prog. Oceanogr. **116**: 179–192. doi:10.1016/j.pocean.2013.07.006

Weber, T., J. A. Cram, S. W. Leung, T. DeVries, and C. Deutsch. 2016. Deep ocean nutrients imply large latitudinal variation in particle transfer efficiency. Proc. Natl. Acad. Sci. USA **113**: 8606–8611. doi:10.1073/pnas.1604414113

Weingartner, T. J., S. L. Danielson, and T. C. Royer. 2005. Freshwater variability and predictability in the Alaska Coastal Current. Deep-Sea Res. II: Top. Stud. Oceanogr. **52**: 169–191. doi:10.1016/j.dsr2.2004.09.030

Welschmeyer, N. A., S. Strom, R. Goericke, G. DiTullio, M. Belvin, and W. Petersen. 1993. Primary production in the subarctic Pacific Ocean: Project SUPER. Prog. Oceanogr. **32**: 101–135. doi:10.1016/0079-6611(93)90010-B

Williams, R. G., V. Roussenov, and M. J. Follows. 2006. Nutrient streams and their induction into the mixed layer. Glob. Biogeochem. Cycles **20**: 102756. doi:10.1029/2005GB002586

Wilson, S. E., D. K. Steinberg, and K. O. Buesseler. 2008. Changes in fecal pellet characteristics with depth as indicators of zooplankton repackaging of particles in the mesopelagic zone of the subtropical and subarctic North Pacific Ocean. Deep-Sea Res. II: Top. Stud. Oceanogr. **55**: 1636–1647. doi:10.1016/j.dsr2.2008.04.019

Yingling, N., T. B. Kelly, T. A. Shropshire, M. R. Landry, K. E. Selph, A. N. Knapp, S. A. Kranz, and M. R. Stukel. 2022. Taxon-specific phytoplankton growth, nutrient utilization and light limitation in the oligotrophic Gulf of Mexico. J. Plankton Res. **44**: 656–676. doi:10.1093/plankt/fbab028

Acknowledgments

We thank the Captain and crew of the R/V *Sikuliaq*, the science party on the 2019 Summer Northern Gulf of Alaska Long Term Ecological Research program (NGA-LTER) Process cruise, and Catherine Fuller, NOAA Teacher at Sea, for assistance with sample collection. We also thank Colleen Durkin for discussions of polyacrylamide gel image analyses and the two reviewers for their constructive comments. Funding for this effort was provided by NSF Northern Gulf of Alaska-LTER grant number 1656070 and NSF CAREER Award grant number 1654663.

Conflict of Interest

None declared.

Submitted 18 May 2023
Revised 12 March 2024
Accepted 17 March 2024

Associate editor: Anja Engel